Biophysics of disordered nuclear receptors and their DNA binding regulation

Heling, L.W.H.J.

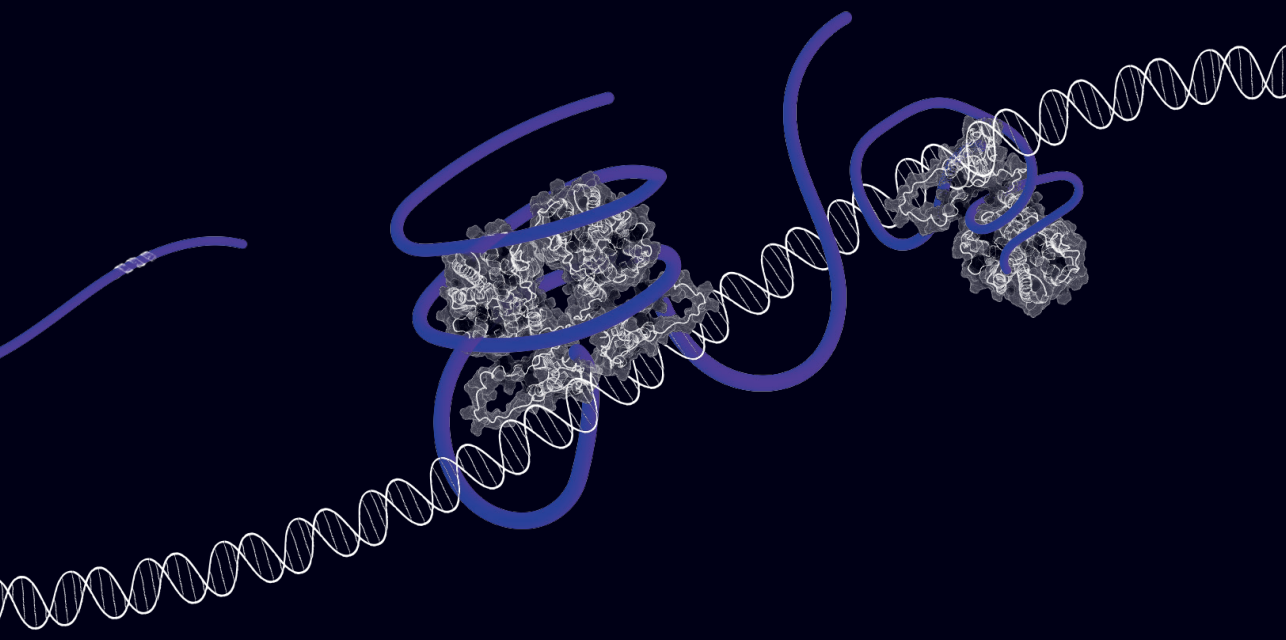

Chapter 4

Modulation of Nur77–DNA Interactions by the Glucocorticoid Receptor

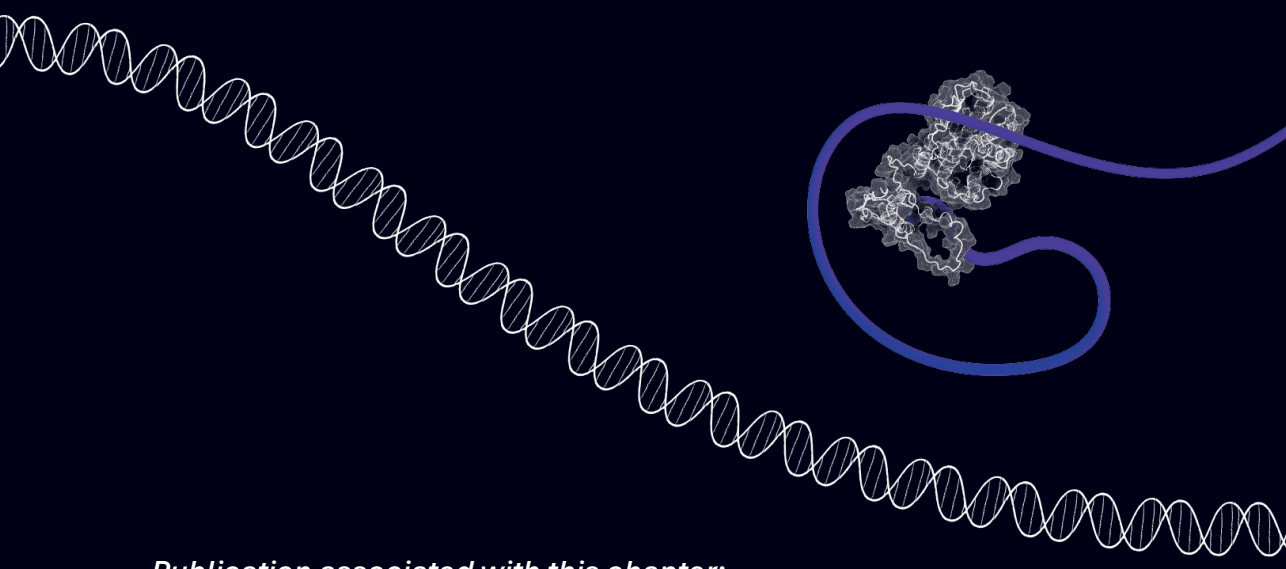

Publication associated with this chapter:

Laurens W. H. J. Heling, Kristina Kovač, Carlie J.M. de Vries, Alireza Mashaghi. *Modulation of Nur77–DNA Interactions by the Glucocorticoid Receptor.* Biochem J **483**(4): 429–440 (2026).

Abstract

Nuclear receptors (NRs) comprise a superfamily of (ligand-)regulated transcription factors that are pivotal in orchestrating gene networks essential for development, metabolism, and cellular homeostasis. Their activity is critical for normal physiology—and consequently—dysregulation of NR signalling is implicated in a wide array of human diseases. Within the superfamily, the orphan nuclear receptor Nur77 and the glucocorticoid receptor (GR) are key regulators that exhibit significant, primarily antagonistic, crosstalk, crucial for modulating inflammatory and stress responses. Despite the recognised importance of their interplay, the precise molecular mechanisms by which GR modulates Nur77's engagement with DNA remain incompletely defined. This study elucidates the direct impact of GR and its ligand, dexamethasone (Dex), on the DNA binding dynamics of Nur77. Single-molecule DNA tightrope assays revealed that Nur77 employs a three-dimensional diffusion-based search mechanism on non-specific DNA, characterised by transient interactions with two distinct dissociation kinetic profiles. GR significantly stabilises Nur77–DNA interactions, evidenced by a shift towards longer residence times, primarily achieved by slowing the dissociation of the more transiently interacting Nur77 population. Conversely, single-molecule and biochemical assays demonstrated that Dex alone markedly reduces Nur77's overall DNA binding affinity kinetics and frequency in a sequence-dependent manner, to such an extent that accurate quantification was unfeasible. These findings delineate distinct modulatory effects of the GR protein and its ligand on Nur77–DNA interactions, providing crucial biophysical insights into their complex regulatory interplay and revealing a direct, GR-independent impact of dexamethasone on Nur77's DNA engagement.

Introduction

Nuclear receptors (NRs) constitute a superfamily of 48 transcription factors essential for regulating gene networks governing development, metabolism, cellular homeostasis, and immune response[1–3]. Dysregulation of NR signalling is implicated in numerous pathologies[4–6]. Among these, the orphan nuclear receptor Nur77 (NR4A1/TR3/NGFIB) is a key regulator whose activity is intricately linked to other NRs. A prominent example is the glucocorticoid receptor (GR, NR3C1), a central mediator of stress responses and inflammation[7,8].

Nur77 belongs to the NR4A subfamily and possesses a canonical NR architecture **(Figure 1A)** with a large intrinsically disordered N-terminal activation domain **(Figure 1B)** and well-structured DNA binding (DBD) and ligand binding domains (LBD) **(Figure 1B and 1C)**. As an orphan receptor, Nur77 exhibits unique regulatory features, necessitated by the ligand-binding pocket of the LBD being largely occluded by bulky hydrophobic residues. Despite this structural barrier, a growing list of compounds has been identified that may modulate Nur77[9–13]. However, the underlying functional mechanisms remain unclear, and there is no consensus regarding the therapeutic potential of these compounds[14]. Consequently, Nur77 activity is thought to be governed primarily by alternative factors such as its expression level, post-translational modifications (PTMs) predominantly located in the NTD **(Figure 1B)**, and crucial protein–protein interactions (PPIs), rather than conventional ligand binding[15–17]. As an immediate-early gene, Nur77 expression is rapidly induced by diverse stimuli, allowing it to quickly influence cellular processes[7,16,17]. Once expressed, Nur77 engages with specific recognition sequences in the genome to modulate target gene expression. It plays versatile roles in fundamental processes including apoptosis, metabolism, and immune function[7,18–20]. Furthermore, Nur77 has been identified as a critical modulator in vascular pathobiology and has been shown to be involved in several pathologies including atherosclerosis by influencing inflammation, vascular cell fate, and lipid metabolism[21–26]. Understanding the mechanisms controlling its interactions with DNA is thus key to deciphering its diverse cellular functions.

The GR, a well-characterised steroid-activated receptor, acts as one of the key interaction partners influencing Nur77 activity[8,27]. Upon ligand binding, GR mediates widespread changes in gene expression through nuclear translocation and interactions with chromatin, co-regulators, and other transcription factors, exerting both activating and potent repressive effects, notably contributing to immune suppression[28,29]. Given the overlapping physiological roles and regulatory inputs for Nur77 and GR, their direct interplay represents a significant control point.Significant crosstalk, predominantly antagonistic, exists between Nur77 and GR[17,27]. Glucocorticoids, acting via GR, can dampen Nur77 signalling both by partially inhibiting Nur77 gene induction and by directly antagonizing Nur77 protein activity[17,27,30,31]. This antagonism involves direct PPIs mediated through their respective DNA-binding domains (DBDs) [27]. Classic examples, such as the regulation of the

pro-opiomelanocortin (POMC) gene, illustrate this interplay where GR represses Nur77-driven transcription, potentially via recruitment to Nur77-occupied sites[17,27]. Moreover, GR activation can broadly influence Nur77's association with chromatin, as suggested by studies on targets like the steroidogenic acute regulatory protein (StAR) gene[32]. These interactions form a critical regulatory node with consequences for hypothalamic–pituitary–adrenal (HPA) axis feedback and immune cell modulation[30,33].

Despite the established direct interaction, precisely how this association with GR modulates Nur77's broader engagement with DNA remains incompletely understood. Does the GR–Nur77 interaction lead to a general inhibition of Nur77's DNA binding affinity or stability, or does it subtly reshape Nur77's genomic interactions and transcriptional potential across diverse chromatin contexts? The mechanisms dictating how the physical interaction translates into altered DNA occupancy and function—whether through steric effects, altered protein conformation, cofactor modulation, or PTM interplay—require further elucidation[17,27,34]. A key gap lies in understanding the global impact of GR on Nur77's DNA binding landscape. We hypothesise that the direct interaction with GR alters the fundamental DNA binding properties of Nur77, influencing its overall genomic distribution and transcriptional capacity.

This study aims to dissect the molecular consequences of the GR–Nur77 interaction on Nur77's general DNA binding behaviour. Using a combination of single-molecule DNA tightrope and biophysical approaches, we investigate how complex formation with GR modulates Nur77's association with DNA in a simple model system. Furthermore, we mapped the impact of a potent synthetic corticosteroid, dexamethasone (Dex) on Nur77. Our results reveal direct modulation by GR and Dex on Nur77–DNA interactions, providing crucial insights on Nur77 regulation.

Materials and methods

Nur77 expression and purification

Sf9 cells were cultured to a density of 1.5×10^6 cells/ml (500 ml) and infected with baculovirus encoding human Nur77 with a N-terminal histidine-tag. The cells were harvested after three days through centrifugation. The pellet underwent 2 freeze/thaw cycles in liquid nitrogen and a water bath at 40°C. After freezing the cells for the third time, the cells were thawed in 40 ml lysis buffer (20 mM HEPES-KOH, pH 8; 1 M KCl; 10 mM Imidazole, pH 8; 100 mM L-arginine; 0.5% IGEPAL; 10% glycerol and fresh EDTA-free protease inhibitors). The viscous lysate was passed through a 21G needle 6 times to shear the DNA (or until the lysate became less viscous). The lysate was divided into 1.5 ml tubes and centrifuged for 40 min, 13k rpm, at 4°C. Ni-NTA beads (5 ml) were washed twice with demineralised water and twice with wash buffer (20 mM HEPES-KOH, pH 8; 1 M KCl; 20 mM Imidazole, pH 8; 100 mM L-arginine; 0.5% IGEPAL; 10% glycerol and freshly added PMSF). The lysate

was applied to the beads and incubated for 3 hours at room temperature. Supernatant was removed after mild centrifugation and beads were washed 3x (4–5x column volume) with wash buffer. The beads were then transferred to a 20ml column and elution was performed with 3 ml elution buffer (20 mM HEPES-KOH, pH 8; 1 M KCl; 100 mM L-arginine; 500 mM Imidazole, pH 8; 0.5% IGEPAL; 10% glycerol; PMSF added fresh). Elution was monitored with 1x Bradford reagent (60 µl 1x Bradford and 1.5 µl sample because of the presence of L-arginine) **(Figure S1)**. Proteins were aliquoted, flash frozen in liquid nitrogen and stored at -80°C.

Microscale thermophoresis (MST)

A fluorescently labelled duplex DNA (fDNA) lacking a Nur77 recognition site was used as a substrate. The top strand was 31 base pairs long **(Table S1)**, while the bottom strand was 32 base pairs long, creating an overhang on the 5' end of the duplex. This overhang was filled with an aminoallyl-dUTP-ATTO-647N (NU-803-647N-S, Jena Bioscience) using DNA Polymerase I, Large (Klenow) Fragment (M0210, New England Biolabs). The reaction was cleaned up using the Monarch® Spin PCR & DNA Cleanup Kit (T1130, England Biolabs) to remove free nucleotides. The fDNA substrate was checked for homogeneity on a 2% agarose gel. Nur77 proteins were dialysed in imaging buffer (100 mM Tris-HCl (pH 7.5), 100 mM NaCl, 20 mM $MgCl_2$) overnight before being diluted from 500 nM to 2.92 nM in imaging buffer supplemented with 0.4% Tween-20 and optionally 50 nM Dexamethasone (D1756, Sigma Aldrich). These samples were mixed 1:1 with the 80 nM of the fDNA substrate in milliQ water to ensure all samples contained 40nM fDNA and Nur77 at concentrations ranging from 250 nM to 1.46 nM in 50 mM Tris-HCl (pH 7.5), 50 mM NaCl, 10 mM $MgCl_2$, 0.2% Tween-20 with or without Dexamethasone., Each sample was incubated at room temperature for 10 minutes and transferred into MST capillaries (Standard Monolith Capillaries, MO-K022, NanoTemper, Germany). MST measurements were done on a Monolith NT.115 instrument (NanoTemper, Germany) at 40% LED power and medium MST power. Total measurement time was 30s, with 5s laser off, 20s laser on and 5s laser off. F_{norm} values were evaluated after 10s of laser on and normalised against baseline (DNA alone).

Single-molecule DNA tightrope assay

The DNA tightrope assay was described previously in detail[35,36]. In short, a custom microfluidic flow chamber was made by combining a standard microscope slide with two holes drilled in it, a double-sided tape gasket and a silanised coverslip. Two tubes connected to a syringe on a peristaltic pump (World Precision Instruments AL1000-220) and a custom Eppendorf tube enabled controlled movement of reagents through the flow chamber. To reduce non-specific surface interactions of proteins, DNA or fluorophores, the flow chamber was blocked by overnight incubation in mPEG buffer (25 mg/ml mPEG5000 in 250 mM $NaHCO_3$, pH 8.2) followed by incubation overnight in ABT buffer (10 mg/ml BSA, 0.1% Tween-20 & 0.1% NaN_3). After careful washing of the flow chamber with buffer, 5 µm silica microspheres (Bang's Laboratories, USA) coated with poly-L-lysine

(P5899, Sigma-Aldrich) are deposited on the surface and -phage DNA (500 ng) is flowed back and forth through the chamber at a constant velocity (300 µL/min) for 40 minutes, elongate the DNA molecules and forming single-molecule DNA tightropes between the beads **(Figure 1D and E)**.

Proteins were labelled with fluorescent Quantum dots. The his-tag located on the Nur77 was tagged through a Qdot antibody sandwich. Nur77 (1 µM) was dialysed against the imaging buffer (described in the MST section) overnight. An equimolar concentration of Hexa-His Primary Antibody (10001-0-AP, Proteintech) was added to the protein and incubated on ice for 30 minutes. A F(ab')2-Goat anti-Mouse IgG (H+L) Secondary Antibody with a 525 Qdot (Q-11041MP, Invitrogen) at was then added to the protein:primary antibody solution at a 3:1 excess (to ensure single labelled Qdots) and incubated for 30 minutes on ice. Labelled proteins were diluted in imaging buffer, and prepared for introduction into the tightrope assay. The final concentration of Nur77 was in the assay 1 nM, which ensured single-molecule resolution with a limited number of molecules that can interact with each DNA tightrope. The imaging buffer was supplemented with 10 mM DTT, which we found reduced "blinking" of the Qdot, a phenomenon where the emission of the Qdot is temporarily reduced. We incubated Qdots, without protein, into the DNA assay to exclude DNA binding by the Qdots (data not shown).

For experiments with GR, commercially available recombinant full-length human GR (ab82089, Abcam) was activated with dexamethasone to avoid aggregation. This sample was filtered to reduce any present aggregates and aliquoted. 1 nM of dexamethasone activated GR was introduced into the flow chamber via the reservoir tube. For experiments with dexamethasone, 25 nM dexamethasone was introduced to the flow chamber through the reservoir.

Super resolution fluorescence microscopy

Single-molecule imaging was performed on a home-built wide-field setup, based on an Axiovert S100 (Zeiss, Germany) inverted microscope equipped with a 100x 1.4NA oil-immersion objective (Zeiss, Germany) at room temperature (20 °C). The sample was excited by a 488nm laser (Sapphire CDRH, Coherent Inc., USA). The intensity and timing were set through an acousto-optic modulator (AOTFnC-VIS, AA-OptoElectronic, France) such that the intensity was set at 1 kW/cm^2 and the illumination time at 10 ms per frame. The light was detected through a dichroic/emission combination (Di01-R405_488_561_635/zet405_488_561_640m, Semrock, USA). The signal of individual dye molecules was captured on a sCMOS camera (Orca Flash 4.0V2, Hamamatsu, Japan). The comparison of the single-molecule fluorescence signal to background yielded a signal-to-noise ratio of 14 and were spatially distributed according to the microscope's point-spread function (440 nm FWHM), allowing for localisation of individual fluorophores with sub-30 nm precision[37].

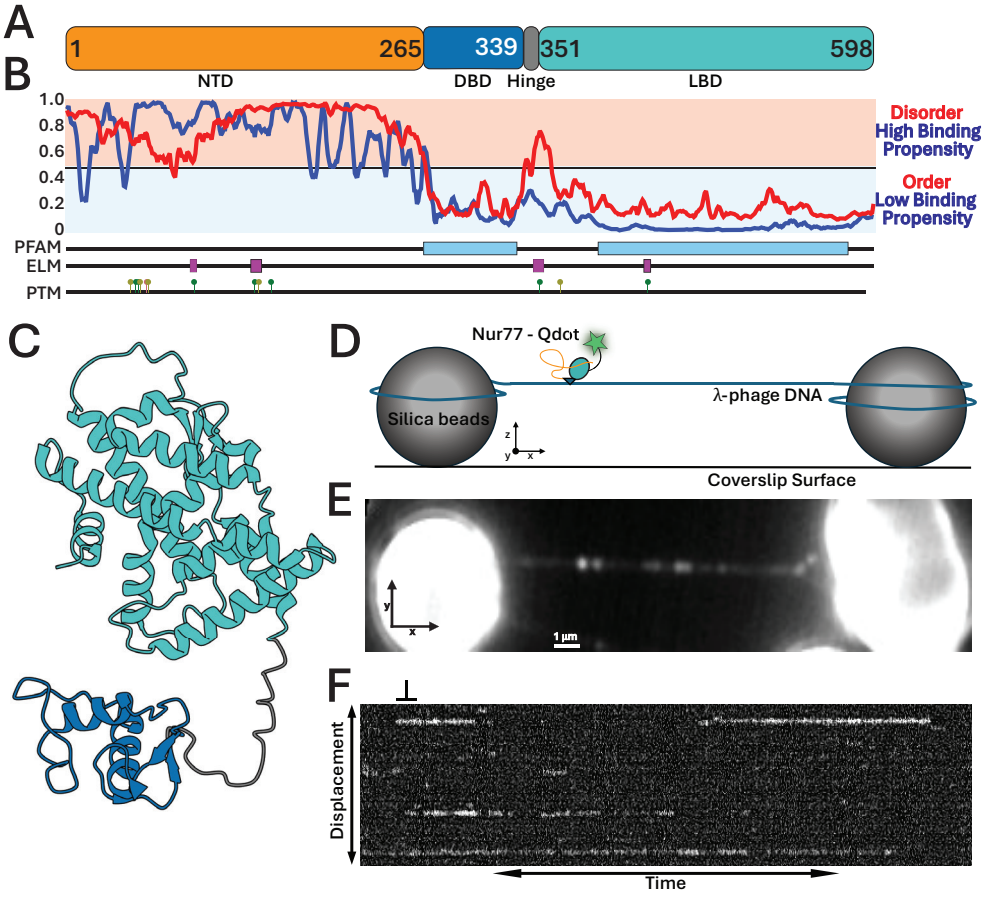

Figure 1. Single-molecule analysis of Nur77 DNA interactions. ***(A)*** *Cartoon of the linear protein structure of Nur77, with the residue numbers depicting the borders of each region. The hinge region is encoded by residue 340 to 350.* ***(B)*** *AIUPred[43,44] (https://aiupred.elte.hu/) plot, depicting the predicted likelihood of residues being more structurally ordered or disordered (red graph), and which residues and regions have a propensity to be functional binding motifs (blue graph, scores >0.5). Underneath the plot are the PFAM domains, the recognised eukaryotic linear motifs (ELM) and low throughput translational modification sites (PTM) noted. The plot is aligned with the linear cartoon from* ***A****.* ***(C)*** *Alphafold 3 derived model of human Nur77 DBD-LBD (Alphafold ID: AF-P22736-F1-v6), colour coded by canonical domain architecture as depicted in* ***A****.* ***(D)*** *Graphical representation of the DNA tightrope assay used to observe single-molecule interactions. Nur77 domains are coloured according to the structure in* ***A****, with the NTD forming a flexible loop as we cannot be certain of its conformation. The Qdot is depicted as a star.* ***(E)*** *A maximum intensity Z-stack projection from a micrograph, illustrating a DNA tightrope stretched between silica beads with bound Nur77 molecules visible as bright spots.* ***(F)*** *Kymographic transformation of a single DNA tightrope revealing Nur77 binding and releasing along the tightrope over time. Scale bar represents 100 ms along the time axis and 0.727 µm along the displacement axis. Abbreviations: NTD: amino-terminal transactivation domain, DBD: DNA binding domain, LBD: ligand binding domain.*

Data acquisition and analysis

For single-molecule microscopy, we prepared three separate flow cells per condition. When a suitable tightrope was detected, 60 second videos were recorded. The videos were converted into kymographs using ImageJ[38]. To identify tightrope positions between beads, videos were projected as Z-stacks using maximum intensity projection. A 25-pixel rolling ball radius background subtraction was applied to the kymographs to average the intensity of bright and dim binding events. Kymograph projections allow the identification of different DNA search mechanisms: proteins sliding along the DNA to search for its target sequences will appear as movement along the y-axis over time, while a 3-dimensional search mechanism is represented by horizontal streaks **(Figure 1F)**. For the lifetime analysis, molecules exhibiting binding exceeding the video length were excluded. To mitigate bin size bias, attached lifetimes were plotted as cumulative frequency histograms and fitted. The necessity of single versus double exponential fits was assessed via F-test. Data fitting was performed with a custom-built Python code, using numpy[39], pandas, matplotlib[40], seaborn[41] and scipy[42] libraries. Additional error analyses were performed in Origin2024 (OriginLab Corporation, USA) to determine fitting errors using the parameters from Python fits. MST data was normalised against DNA alone and plotted using Microsoft Excel. The fitting and k_D calculations were performed using a custom Python script.

Results

Nur77 performs a fast-paced 3D search on DNA

Transcription factors like Nur77 may use a number of search mechanisms to find their target DNA sequence *in vivo*[47]. To directly visualise the search mechanism of Nur77 for a sequence in real-time, we employed the *in vitro* DNA tightrope assay. In this assay, individual DNA molecules are suspended between 5 µm silica beads deposited on a PEGylated surface of a custom-built microfluidic chamber **(Figure 1D)**[35,36]. This allows for the direct observation of protein–DNA interactions where the protein has full accessibility to the DNA while improving signal-to-noise ratios. We labelled individual Nur77 proteins with a bright photostable Qdot via an anti-His-tag antibody conjugation. We incubated Nur77 with lambda-phage (λ) DNA, a long DNA substrate ideal for the tightrope assay **(Figure 1E)**. Two different recognition sequences have been identified for Nur77 *in vivo*, the NurRE (TGATATTTn$_6$AAATGCCA), to which Nur77 binds as a homo- or heterodimer (with other NR4A members), and the NBRE sequence (AAGGTCA) which is bound by Nur77 as a monomer. λ-DNA lacks the full canonical NurRE sequence but does contain a few half NurRE sites as well as some NBRE sites. We observed interactions within a 60 second time window. Videos of Nur77 interactions with DNA were transformed into kymographs **(Figure 1F)**, from which different types of diffusion behaviour can be characterised[36].

Our data revealed that DNA-bound Nur77 did not exhibit any sliding behaviour along the DNA within the spatiotemporal limits of our setup (<30 nm, ~88 bases, 10 ms). The range

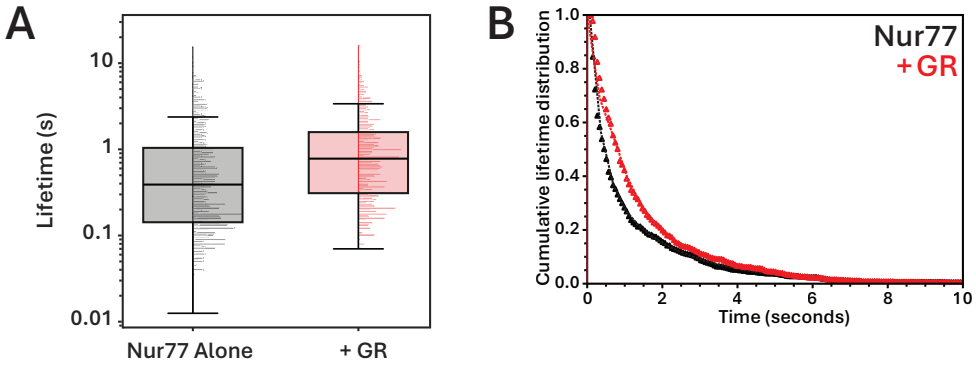

C

	k_{fast} (s^{-1})	Fit error (s^{-1})	k_{slow} (s^{-1})	Fit error (s^{-1})	*n*
Nur77	3.421	0.065	0.542	0.008	809
+ GR	1.521	0.041	0.458	0.013	670

Figure 2. Nur77–DNA interactions dynamics are modulated by GR. (A) *Boxplot with attached normalised histograms of the molecular lifetimes (in seconds) reveal that (Dex activated) GR significantly increases Nur77 lifetimes on DNA (Mann-Whitney U test, $p < 0.001$).* ***(B)*** *Cumulative lifetime distributions of Nur77 interacting with DNA alone (black triangles) and in addition of Dex-activated GR (red troangles. Experimental data fit with a double exponential (black and red dotted lines respectively).* ***(C)*** *The double exponent allows for the extraction of two dissociation rate constants (k_{fast} and k_{slow}) displayed in this table, including the fit error. n represents the number of observations from three separate flow chambers.*

of observed binding lifetimes, from 0.03 to exceeding 15 seconds (n = 809 molecules), aligns with the stochastic nature of molecular dissociation events, and is indicative of a kinetically heterogeneous population. Together these findings indicate that Nur77 probes DNA for its target sequence using three-dimensional diffusion dynamics.

GR shifts lifetime equilibrium to longer lived states.

Upon introduction of equimolar concentrations of (dexamethasone (Dex)-activated) GR, the data indicate a discernible shift towards longer lifetimes. The average lifetime observed for Nur77 with (Dex activated) GR present was 1.32 ± 0.06 seconds, which is markedly longer than the average of 0.98 ± 0.06 seconds for Nur77 alone (apo Nur77). The trend towards longer lifetimes is supported by an examination of the full-range of observed lifetimes **(Figure 2A)**. This distributional shift is further characterised by a notable reduction in the number of events where Nur77 resides on the DNA less than 0.3 seconds, and a concomitant enrichment of species persisting in the 0.5 to 2-second range. Consistent with the right-skewed distributions typical of single-molecule decay, the presence of (Dex activated) GR extended the tail of longer-lived molecules.

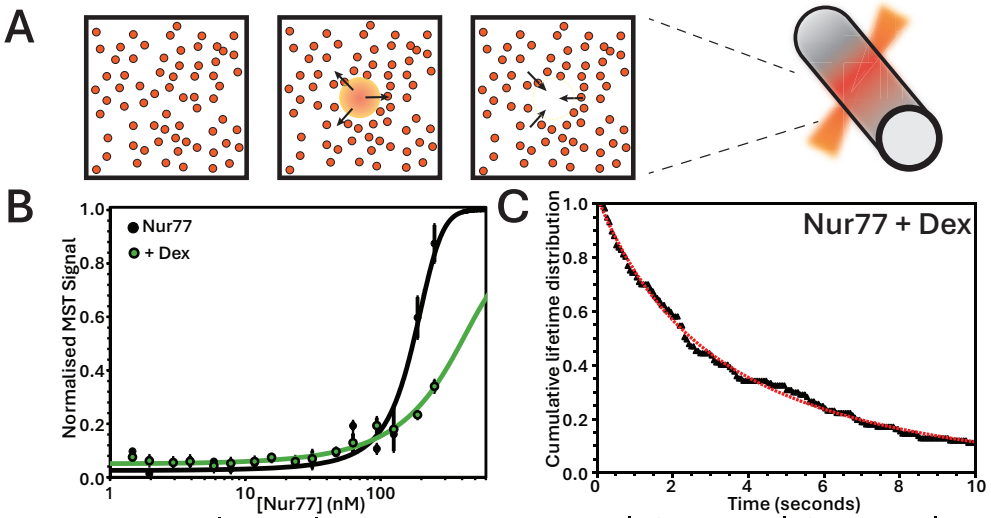

Dex	k_D (nM)	Error (nM)
-	173.46	9.98
+	c.n.d.	c.n.d.

	k_1 (s^{-1})	Fit error (s^{-1})	k_2 (s^{-1})	Fit error (s^{-1})	*n*
+ Dex	0.678	0.059	0.182	0.004	117

Figure 3. Dexamethasone (Dex) alone disrupts Nur77/DNA interactions. (A) *Cartoon representation of an MST assay. The fluorescence emission of the capillary is continuously monitored. Upon application of heat by an infrared laser, molecules diffuse away from this point with a rate constant inversely correlated to their hydrodynamic size.* ***(B)*** *MST of Nur77 titrated against DNA without (black) and with (green) Dex. k_D and error extracted from fitting the MST values with a binding curve are represented in the table below the graph. Means ± S.E.M., n = 6, c.n.d. = k_D cannot reliably be determined.* ***(C)*** *Cumulative lifetime distribution from the single-molecule tightrope assay reveals that the kinetic parameters of Nur77 with Dex is significantly altered. Black triangles represent the data, the red dotted line the double exponential fit. Dissociation rate constants (k_1 and k_2) with fit error in the table below. n represents the number of observations from three separate flow chambers.*

Collectively, these data demonstrate that activated GR alters the molecular dynamics of Nur77 on DNA. This is observed not merely as an extension of a few longer-lived outliers, but rather a comprehensive shift in the entire lifetime distribution.

The dissociation of proteins on DNA can be modelled as a Poisson process[48]. To further elucidate the heterogeneity in residence lifetimes induced by GR, and to extract the rate constants, we plotted the data as cumulative lifetime distributions **(Figure 2B)**. Fitting the data yields the dissociation rate constant (k_{off}). If a system has multiple intermediates, the number of terms fit to the distribution can indicate the number of intermediates. Our data fit best to a double exponential function suggesting the presence of two kinetic intermediates for both apo Nur77 **(Figures 2B, C and S2)** and Nur77 with GR **(Figures 2B,**

C and S3). For apo Nur77, approximately two-thirds of events (63.3%) exhibited short dwell times on DNA, with a k_{off} of 3.421 ± 0.065 s^{-1}, while the population of longer-lived interactions (36.7%) resided at the DNA with a k_{off} of 0.542 ± 0.008 s^{-1} **(Figure 2C)**. In the presence of GR, the distribution between short- and longer-lived populations was similar to apo Nur77 (63.5% and 36.5% respectively), yet the rate constants decreased. While for the longer-lived populations this was only a moderate decrease with a k_{off} of 0.458 ± 0.013 s^{-1}, for the short-lived population the rate constant was halved to 1.521 ± 0.041 s^{-1}.

Dexamethasone disrupts Nur77 DNA binding

The potent synthetic glucocorticoid, dexamethasone (Dex), was added to ensure GR was in its active form. Therefore we conducted additional experiments to understand the direct impact of Dex on Nur77 binding kinetics.

First, we studied the DNA binding of Nur77 using microscale thermophoresis (MST). This technique quantifies molecular interactions by detecting changes in the diffusion of fluorescent molecules within a temperature gradient **(Figure 3A)**. Compared to traditional techniques such as electrophoretic mobility shift assays (EMSA), MST operates in a free solution without the need for immobilisation or gel matrices. In our setup, the DNA, not the protein, is fluorescently labelled. This prevents protein aggregates—which would diffuse slower than free proteins but normally cannot bind DNA—from skewing the results. MST revealed that while the dissociation constant for Nur77 with unspecific DNA is 174.46 ± 9.98 nmol/l, and that modulation by Dex reduced DNA binding. In this condition, a k_D could not reliably be determined **(Figure 3B)**.

Next, to assess the effect of Dex on the kinetic characteristics of Nur77, we introduced it into the DNA tightrope assay. This revealed a similar image as from the MST results, where addition of Dex yielded a profoundly different outcome compared to both apo Nur77 and Nur77 combined with GR **(Figure 3C, S4 and S5)**. Dex modulation suppressed the detection frequency of DNA binding, (117 events compared to 809 events of apo Nur77), and decreased the k_{off} of the residual observable Nur77 **(Figure 3B**, k_1: 0.687 ± 0.059 s^{-1}; k_2: 0.182 ± 0.004 s^{-1}**)**, while inducing a significant population shift towards the longer-lived state (~61% vs. ~37% baseline). As the λ-DNA contains several (partial and native) recognition sites for Nur77, we set out to understand this observed shift better by performing subsequent MST analysis on Nur77 with different DNA constructs **(Table S1)** in the presence of Dex. This revealed that Dex strongly affected the binding of Nur77 to NurRE DNA, while increasing the k_D of Nur77 with NBRE DNA **(Figure S6)**.

Discussion

The mechanism by which the GR influences the DNA binding dynamics of Nur77 is critical in modulating transcriptional responses. Yet the molecular details of this process, and strategies to potentially modulate it, remain elusive. In this study, by combining single-molecule and biophysical analyses, we obtained several key insights that refine our understanding of the interplay between these two key nuclear receptors **(Figure 4)**. Firstly, our direct visualisation of Nur77 on DNA revealed an intrinsic 3D diffusion-based search mechanism on non-specific DNA. This information provides a fundamental update on Nur77, revealing a predominant 'probing' mode rather than extensive linear tracking along the DNA backbone, which may contribute to its ability to rapidly respond to cellular signals by efficiently scanning the genome.

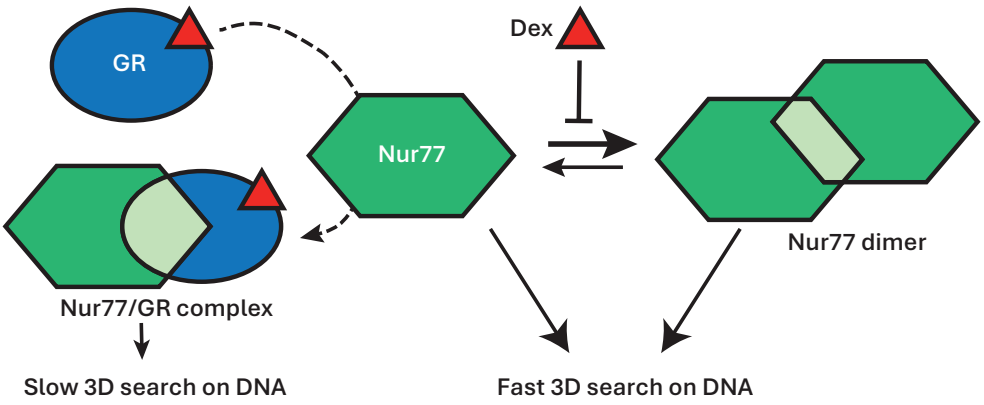

Figure 4. Proposed model for modulation of Nur77–DNA interactions by the glucocorticoid receptor and dexamethasone.

We observed that the DNA interactions of Nur77 are best described through two kinetic populations, a behaviour we have previously identified for the androgen receptor (AR)[49]. *In vivo*, one of the characteristics of Nur77 is its ability to bind DNA as a monomer at the NGFI-B-responsive element (NBRE; AAGGTCA)—unique for a nuclear receptor—as well as a homo- or heterodimer (with other NR4A members) to Nur-responsive elements (NurRE; TGATATTTn$_6$AAATGCCA) in the promoter and enhancer regions of target genes. This versatility underlies the involvement of Nur77 in fundamental processes like apoptosis, metabolism, and immune function[7,19,50]. The λ-phage DNA construct we use in our tightrope assay lacks full sites of the NurRE but does contain a number of half motif sequences as well as a few NBRE-like motifs. The presence of these (half) sites may explain the observation of two populations, where Nur77 bound to a (partial) motif could increase the dwell time on DNA as the presence of specific DNA motifs have been proposed as an explanation for longer dwell times observations of proteins on DNA *in vitro*[51]. Structural studies on other members of the nuclear receptor superfamily (GR and AR) have revealed a DNA probing

mechanism where a monomer binds to half a motif, inducing a conformational change that allows the second monomer to bind[52–54]. Furthermore, for AR, this conformational change induces helicity in the N-terminal domain, enabling co-regulators to interact with the receptor. This structurally links DNA binding to transcriptional regulation[55]. Given the immense size of the genome that these receptors must scan, and the relatively short DNA recognition motifs, it is plausible that this is a common mechanism amongst nuclear receptors, and may be a structural explanation for the population of binding events that we observed. More experiments, including structural elucidation of the Nur77-DBD in complex with DNA, are needed to confirm this model.

We found that the addition of GR significantly alters Nur77–DNA dynamics by markedly stabilizing Nur77. This was evidenced by an increased average residence time, primarily driven by a reduction in the k_{off} of the short-lived interations. This is in line with previous experimental evidence, where direct PPIs lead to repression of Nur77[31]. Since experimental evidence has revealed that GR does not bind to the response elements of Nur77[27], it is more likely that GR physically sequesters Nur77 at other sequences, like the glucocorticoid response elements (GREs; AGAACAn$_3$TGTTCT). As with the NurRE, there are no full GREs within the λ-DNA, though there are approximately 40 half-sites. Such modulation of Nur77's DNA dwell time by the GR protein itself offers a direct biophysical mechanism through which GR could influence the transcriptional output of Nur77. By prolonging Nur77's interaction with DNA, GR might enhance its capacity to engage with co-regulators or the basal transcriptional machinery at specific loci, or conversely, sequester Nur77 at non-productive sites, thereby providing a nuanced means of controlling its activity beyond simple steric hindrance at response elements. Correlating transcription factor binding energetics on DNA with transcriptional output revealed that dwell time is a regulatory factor[56–60], dictated by several variables such as transcription factor concentration, co-regulators, DNA sequence and genome structure.

Our investigation furthermore uncovered a striking direct effect of Dex on Nur77's DNA interactions. Independent of GR, Dex severely attenuated the frequency of Nur77 binding events, while dramatically increasing the stability of DNA binding and shifting the population towards the longer-lived state for those few interactions that did occur. Looking at the differences on different DNA motifs, this kinetic profile suggests that Dex impacts Nur77 by severely hindering its DNA binding ability and/or locking the remaining NBRE bound Nur77 into a hyper-stable (monomeric) conformation. These findings are particularly intriguing, as they suggest that the widely recognised antagonism between GR and Nur77 signalling pathways may be compounded by direct, GR ligand-specific effects on Nur77's fundamental ability to bind DNA. This introduces a previously unappreciated layer of complexity, implying that the cellular concentration and availability of glucocorticoids may directly influence Nur77's genomic targets and residence times, potentially requiring a re-evaluation of glucocorticoid action in Nur77-regulated processes, independent of GR's canonical functions.

In conclusion, we present the first mechanistic characterisation of Nur77–DNA interactions. The combination of real-time single-molecule and biophysical analysis revealed a characteristic behaviour of Nur77, and how this behaviour is affected by another nuclear receptor and a common synthetic glucocorticoid, *in vitro*. Important questions remain, however. Like most nuclear receptors, Nur77 is a complex multidomain protein, whose individual regions serve diverse and context-dependent functions. While structural and functional characterisation of the DBD and LBD of Nur77 exists **(Figure 1C)**, the role of the NTD remains elusive and may provide vital information on the effects of the protein–protein and/or protein–ligand interactions we have observed here. Our approach here reveal fundamental biophysical behaviours of Nur77 binding to DNA using purified proteins, and we recognise that these are not directly translatable to the physiological conditions. Moving forward, the distinct modulatory effects observed *in vitro* require validation within the native cellular environment. Utilizing advanced live-cell imaging techniques (fluorescence correlation spectroscopy (FCS), single-molecule tracking or fluorescence recovery after photobleaching (FRAP)) can assess the nuclear mobility and chromatin residence times of Nur77 under conditions where it interacts with GR or is exposed solely to dexamethasone. It will also be important to see if there is a concentration dependent effect of dexamethasone. Furthermore. given the increasing evidence that transcription factors operate within biomolecular condensates to organise transcription[61], it will be important to investigate the formation and dynamics of Nur77-containing condensates, and whether this is influenced by GR–Nur77 interactions, other nuclear hormone receptors, or by the specific presence of dexamethasone. These experiments will determine if the biophysical mechanisms we describe here translate into functional changes in gene expression regulation within chromatin.

Acknowledgements

We thank Thomas Schmidt (Universiteit Leiden) for providing access, technical assistance and discussions for the single-molecule fluorescence microscopy experiments and the Macromolecular biochemistry group at the Leiden Institute for Chemistry for access and technical assistance to the Microscale Thermophoresis facilities.

Author Contributions

Laurens W. H. J. Heling: Conceptualisation; investigation; methodology; visualisation; formal analysis; data curation; validation; writing–original draft; writing–review and editing. **Kristina Kovač:** Investigation, methodology. **Carlie J.M. de Vries:** Writing–review and editing; resources; investigation. **Alireza Mashaghi:** Conceptualisation; investigation; resources; supervision; project administration; writing–review and editing; writing–original draft; funding acquisition.

References

1. Taubenheim, J., Kortmann, C. & Fraune, S. Function and evolution of nuclear receptors in environmental-dependent postembryonic development. *Front Cell Dev Biol* **9**, 653792 (2021).

2. Frigo, D. E., Bondesson, M. & Williams, C. Nuclear receptors: from molecular mechanisms to therapeutics. *Essays in biochemistry* **65**, 847–856 (2021).

3. Scholtes, C. & Giguère, V. Transcriptional control of energy metabolism by nuclear receptors. *Nat Rev Mol Cell Biol* **23**, 750–770 (2022).

4. Mangelsdorf, D. J. *et al*. The nuclear receptor superfamily: The second decade. *Cell* **83**, (1995).

5. Huang, P., Chandra, V. & Rastinejad, F. Structural overview of the nuclear receptor superfamily: insights into physiology and therapeutics. *Annu Rev Physiol* **72**, 247–272 (2010).

6. Agrawal, S., He, J. C. & Tharaux, P.-L. Nuclear receptors in podocyte biology and glomerular disease. *Nat Rev Nephrol* **17**, 185–204 (2021).

7. Pearen, M. A. & Muscat, G. E. O. Minireview: Nuclear hormone receptor 4A signaling: implications for metabolic disease. *Mol Endocrinol* **24**, 1891–1903 (2010).

8. Chrousos, G. P. The hypothalamic-pituitary-adrenal axis and immune-mediated inflammation. *N Engl J Med* **332**, 1351–1362 (1995).

9. Chintharlapalli, S. *et al*. Activation of Nur77 by selected 1,1-bis(3'-indolyl)-1-(p-substituted phenyl)methanes induces apoptosis through nuclear pathways. *Journal of Biological Chemistry* **280**, (2005).

10. Zhan, Y. *et al*. Cytosporone B is an agonist for nuclear orphan receptor Nur77. *Nat Chem Biol* **4**, (2008).

11. Vinayavekhin, N. & Saghatelian, A. Discovery of a protein-metabolite interaction between unsaturated fatty acids and the nuclear receptor Nur77 Using a metabolomics approach. *J Am Chem Soc* **133**, (2011).

12. Hu, M. *et al*. Celastrol-Induced Nur77 Interaction with TRAF2 Alleviates Inflammation by Promoting Mitochondrial Ubiquitination and Autophagy. *Mol Cell* **66**, (2017).

13. Lakshmi, S. P., Reddy, A. T., Banno, A. & Reddy, R. C. Molecular, chemical, and structural characterization of prostaglandin A2 as a novel agonist for Nur77. *Biochemical Journal* **476**, (2019).

14. Safe, S., Shrestha, R. & Mohankumar, K. Orphan nuclear receptor 4A1 (NR4A1) and novel ligands. *Essays Biochem* **65**, 877–886 (2021).

15. Flaig, R., Greschik, H., Peluso-Iltis, C. & Moras, D. Structural basis for the cell-specific activities of the NGFI-B and the Nurr1 ligand-binding domain. *J Biol Chem* **280**, 19250–19258 (2005).

16. Safe, S. *et al*. Nuclear receptor 4A (NR4A) family - orphans no more. *J Steroid Biochem Mol Biol* **157**, 48–60 (2016).

17. Kurakula, K., Koenis, D. S., van Tiel, C. M. & de Vries, C. J. M. NR4A nuclear receptors are orphans but not lonesome. *Biochim Biophys Acta* **1843**, 2543–2555 (2014).

18. Maxwell, M. A. & Muscat, G. E. O. The NR4A Subgroup: Immediate Early Response Genes with Pleiotropic Physiological Roles. *Nucl Recept Signal* **4**, (2006).

19. McMorrow, J. P. & Murphy, E. P. Inflammation: a role for NR4A orphan

nuclear receptors? *Biochem Soc Trans* **39**, 688–693 (2011).

20. Lith, S. C. *et al*. Nuclear receptor Nur77 regulates immunomechanics of macrophages. *Eur J Cell Biol* **103**, 151419 (2024).

21. Pei, L., Castrillo, A., Chen, M., Hoffmann, A. & Tontonoz, P. Induction of NR4A orphan nuclear receptor expression in macrophages in response to inflammatory stimuli. *Journal of Biological Chemistry* **280**, 29256–29262 (2005).

22. Koenis, D. S. *et al*. Nuclear receptor Nur77 limits the macrophage inflammatory response through transcriptional reprogramming of mitochondrial metabolism. *Cell Rep* **24**, 2127–2140 (2018).

23. Hamers, A. A. J. *et al*. Bone marrow–specific deficiency of nuclear receptor Nur77 enhances atherosclerosis. *Circ Res* **110**, 428–438 (2012).

24. Bonta, P. I. *et al*. Nuclear receptors Nur77, Nurr1, and NOR-1 expressed in atherosclerotic lesion macrophages reduce lipid loading and inflammatory responses. *Arterioscler Thromb Vasc Biol* **26**, 2288 (2006).

25. Auffray, C. *et al*. Monitoring of blood vessels and tissues by a population of monocytes with patrolling behavior. *Science (1979)* **317**, 666–670 (2007).

26. Hanna, R. N. *et al*. NR4A1 (Nur77) deletion polarizes macrophages toward an inflammatory phenotype and increases atherosclerosis. *Circ Res* **110**, 416–427 (2012).

27. Martens, C., Bilodeau, S., Maira, M., Gauthier, Y. & Drouin, J. Protein-protein interactions and transcriptional antagonism between the subfamily of NGFI-B/Nur77 orphan nuclear receptors and glucocorticoid receptor. *Molecular Endocrinology* **19**, (2005).

28. Vandevyver, S., Dejager, L., Tuckermann, J. & Libert, C. New insights into the anti-inflammatory mechanisms of glucocorticoids: an emerging role for glucocorticoid-receptor-mediated transactivation. *Endocrinology* **154**, 993–1007 (2013).

29. Glass, C. K. & Saijo, K. Nuclear receptor transrepression pathways that regulate inflammation in macrophages and T cells. *Nat Rev Immunol* **10**, 365–376 (2010).

30. Okabe, T., Takayanagi, R., Adachi, M., Imasaki, K. & Nawata, H. Nur77, a member of the steroid receptor superfamily, antagonizes negative feedback of ACTH synthesis and secretion by glucocorticoid in pituitary corticotrope cells. *Journal of Endocrinology* **156**, (1998).

31. Philips, A. *et al*. Antagonism between Nur77 and glucocorticoid receptor for control of transcription. *Mol Cell Biol* **17**, 5952–5959 (1997).

32. Martin, L. J. & Tremblay, J. J. Glucocorticoids antagonize cAMP-induced Star transcription in Leydig cells through the orphan nuclear receptor NR4A1. *J Mol Endocrinol* **41**, 165–175 (2008).

33. Mittelstadt, P. R., Taves, M. D. & Ashwell, J. D. Glucocorticoids Oppose Thymocyte Negative Selection by Inhibiting Helios and Nur77. *J Immunol* **203**, 2163–2170 (2019).

34. Anbalagan, M., Huderson, B., Murphy, L. & Rowan, B. G. Post-translational modifications of nuclear receptors and human disease. *Nucl Recept Signal* **10**, e001 (2012).

35. Springall, L., Inchingolo, A. V. & Kad, N. M. DNA-protein interactions studied directly using single molecule fluorescence imaging of quantum dot tagged proteins moving on DNA

tightropes. in *Methods in Molecular Biology* vol. 1431 141–150 (2016).

36. Kad, N. M., Wang, H., Kennedy, G. G., Warshaw, D. M. & Van Houten, B. Collaborative Dynamic DNA Scanning by Nucleotide Excision Repair Proteins Investigated by Single- Molecule Imaging of Quantum-Dot-Labeled Proteins. *Mol Cell* **37**, (2010).

37. Hohng, S. & Ha, T. Near-complete suppression of quantum dot blinking in ambient conditions. *J Am Chem Soc* **126**, 1324–1325 (2004).

38. Schmidt, T., Schütz, G. J., Baumgartner, W., Gruber, H. J. & Schindler, H. Imaging of single molecule diffusion. *Proceedings of the National Academy of Sciences* **93**, 2926–2929 (1996).

39. Schneider, C. A., Rasband, W. S. & Eliceiri, K. W. NIH Image to ImageJ: 25 years of image analysis. *Nat Methods* **9**, 671–675 (2012).

40. Harris, C. R. *et al.* Array programming with NumPy. *Nature* **585**, 357–362 (2020).

41. Hunter, J. D. Matplotlib: A 2D graphics environment. *Comput Sci Eng* **9**, (2007).

42. Waskom, M. seaborn: statistical data visualization. *J Open Source Softw* **6**, (2021).

43. Virtanen, P. *et al.* SciPy 1.0: fundamental algorithms for scientific computing in Python. *Nat Methods* **17**, (2020).

44. Erdős, G. & Dosztányi, Z. AIUPred: combining energy estimation with deep learning for the enhanced prediction of protein disorder. *Nucleic Acids Res* **52**, 176–181 (2024).

45. Erdős, G., Deutsch, N. & Dosztányi, Z. AIUPred – Binding: Energy Embedding to Identify Disordered Binding Regions. *J Mol Biol* **437**, 169071 (2025).

46. Sehnal, D. *et al.* Mol* Viewer: modern web app for 3D visualization and analysis of large biomolecular structures. *Nucleic Acids Res* **49**, W431–W437 (2021).

47. von Hippel, P. H. & Berg, O. G. Facilitated target location in biological systems. *J Biol Chem* **264**, 675–678 (1989).

48. Ghodke, H. *et al.* Single-molecule analysis reveals human UV-damaged DNA-binding protein (UV-DDB) dimerizes on DNA via multiple kinetic intermediates. *Proceedings of the National Academy of Sciences* **111**, E1862–E1871 (2014).

49. Heling, L. W. H. J. *et al.* Deciphering the allosteric control of androgen receptor DNA binding by its disordered N-terminal domain. *Mol Cell Endocrinol* **608**, 112634 (2025).

50. Lith, S. C. & de Vries, C. J. M. Nuclear receptor Nur77: its role in chronic inflammatory diseases. *Essays Biochem* **65**, 927–939 (2021).

51. Hettich, J. & Gebhardt, J. C. M. Transcription factor target site search and gene regulation in a background of unspecific binding sites. *J Theor Biol* **454**, (2018).

52. Lee, X. Y. *et al.* Structural mechanism underlying variations in DNA binding by the androgen receptor. *J Steroid Biochem Mol Biol* **241**, 106499 (2024).

53. Frank, F., Ortlund, E. A. & Liu, X. Structural insights into glucocorticoid receptor function. *Biochem Soc Trans* **49**, 2333–2343 (2021).

54. Meijsing, S. H. *et al.* DNA Binding Site Sequence Directs Glucocorticoid Receptor Structure and Activity. *Science (1979)* **324**, 407–410 (2009).

55. Brodie, J. & McEwan, I. J. Intra-domain communication between the N-terminal and DNA-binding domains of the androgen receptor: modulation

of androgen response element DNA binding. *J Mol Endocrinol* **34**, 603–615 (2005).

56. Chen, T.-Y. *et al*. Concentration-and chromosome-organization-dependent regulator unbinding from DNA for transcription regulation in living cells. *Nat Commun* **6**, 7445 (2015).

57. Bain, D. L. *et al*. Glucocorticoid Receptor–DNA Interactions: Binding Energetics Are the Primary Determinant of Sequence-Specific Transcriptional Activity. *J Mol Biol* **422**, 18–32 (2012).

58. Clauß, K. *et al*. DNA residence time is a regulatory factor of transcription repression. *Nucleic Acids Res* **45**, 11121–11130 (2017).

59. Auble, D. T., Wang, D., Post, K. W. & Hahn, S. Molecular analysis of the SNF2/SWI2 protein family member MOT1, an ATP-driven enzyme that dissociates TATA-binding protein from DNA. *Mol Cell Biol* **17**, 4842–4851 (1997).

60. Stavreva, D. A., Müller, W. G., Hager, G. L., Smith, C. L. & McNally, J. G. Rapid glucocorticoid receptor exchange at a promoter is coupled to transcription and regulated by chaperones and proteasomes. *Mol Cell Biol* **24**, 2682–2697 (2004).

61. Stortz, M., Presman, D. M. & Levi, V. Transcriptional condensates: a blessing or a curse for gene regulation? *Commun Biol* **7**, 187 (2024).

Supplementary Material

Table S1. DNA sequences used in MST

DNA Substrate	Sequence (5’ - 3’)
Non-specific	CCAAAGAAGAGAATTAAGAGCACGCAAAGG
NBRE	GGGCGGCGAA**AAGGTCA**CCTGAATCGC
NurRE	GGGCGGCGA**TGATATTT**GAGAAT**AAATGCCA**CCTGCGCGC

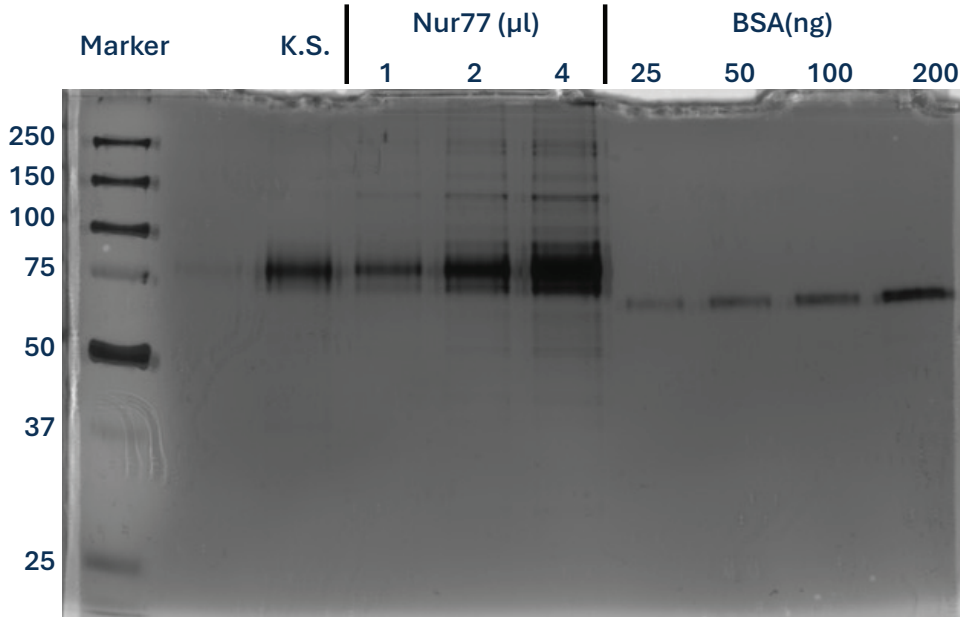

Figure S1. 10% SDS-PAGE Coomassie-stained gel of purified Nur77 samples. *This gel was used to analyse the purity and concentration of Nur77. Increasing volumes (1, 2, and 4 µl) of the Nur77 sample were loaded alongside a known sample of Nur77 (K.S.) and a quantitative Bradford protein assay standard curve of Bovine Serum Albumin (BSA) (25, 50, 100, and 200 ng). Concentration of Nur77 was determined to be 211 ng/µl. The leftmost lane contains a molecular weight ladder.*

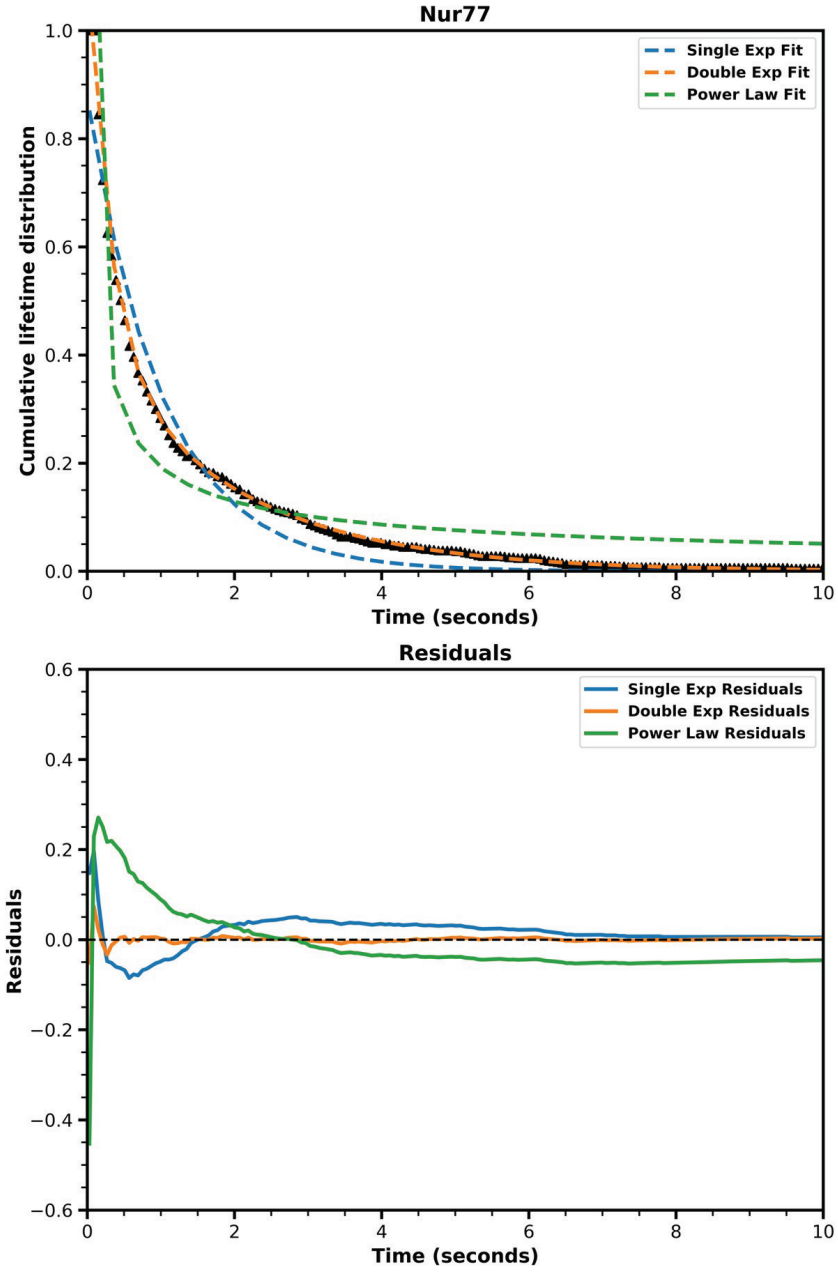

Figure S2. Single exponential, double exponential and power law fitted to cumulative lifetime distributions, with residuals plots of Nur77 alone. *Black triangles represent the data, blue dotted line the single exponential fit, the orange dotted line the double exponential fit, green dotted line the power law fit.*

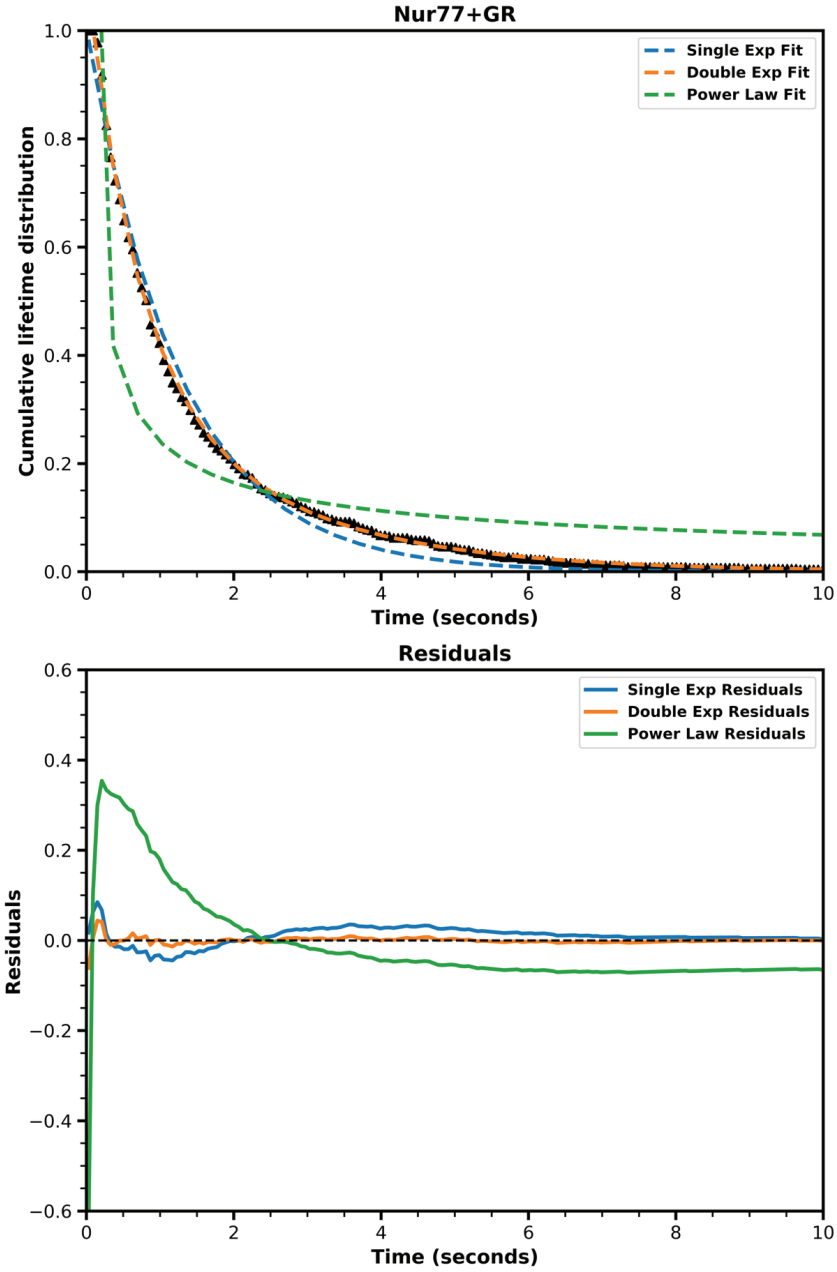

Figure S3. Single exponential, double exponential and power law fitted to cumulative lifetime distributions, with residuals plots of Nur77 with the glucocorticoid receptor. *Black triangles represent the data, blue dotted line the single exponential fit, the orange dotted line the double exponential fit, green dotted line the power law fit.*

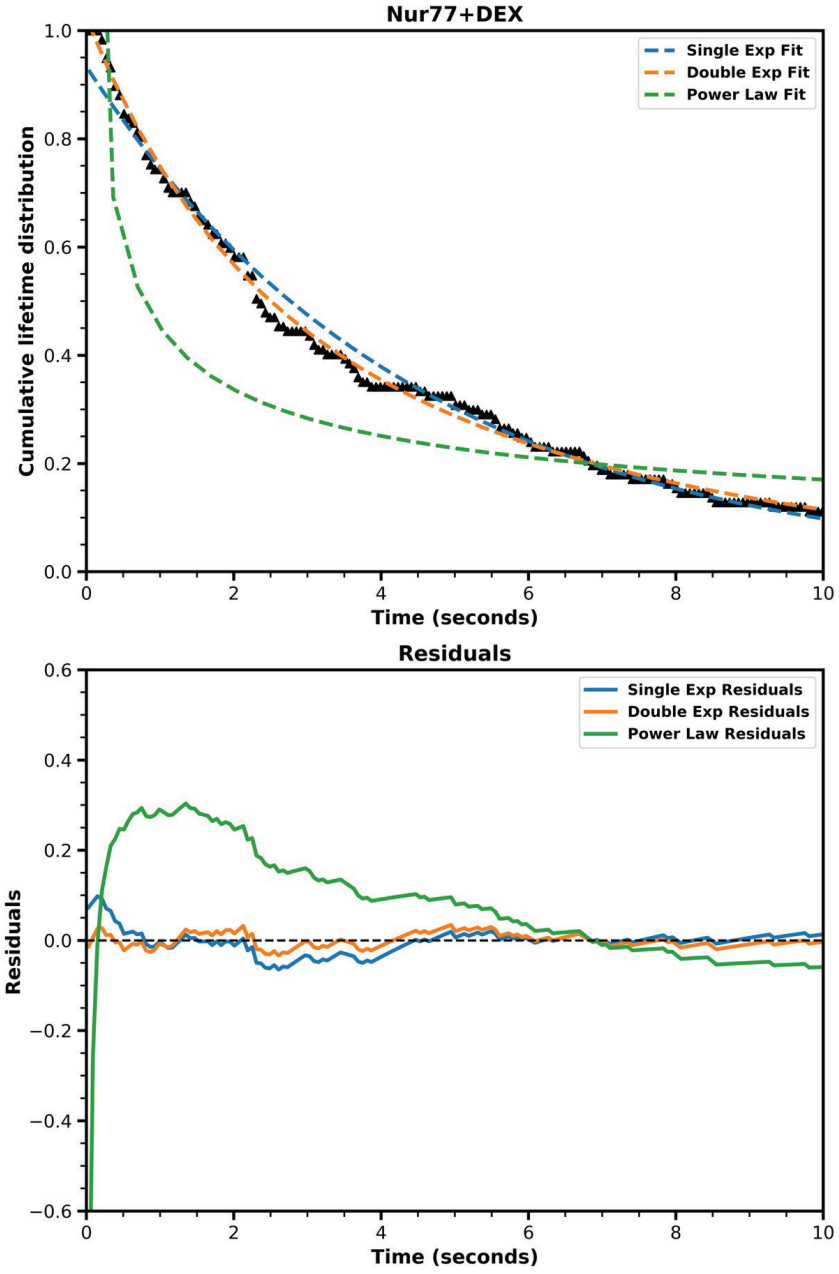

Figure S4. Single exponential, double exponential and power law fitted to cumulative lifetime distributions, with residuals plots of Nur77 with dexamethasone. *Black triangles represent the data, blue dotted line the single exponential fit, the orange dotted line the double exponential fit, green dotted line the power law fit.*

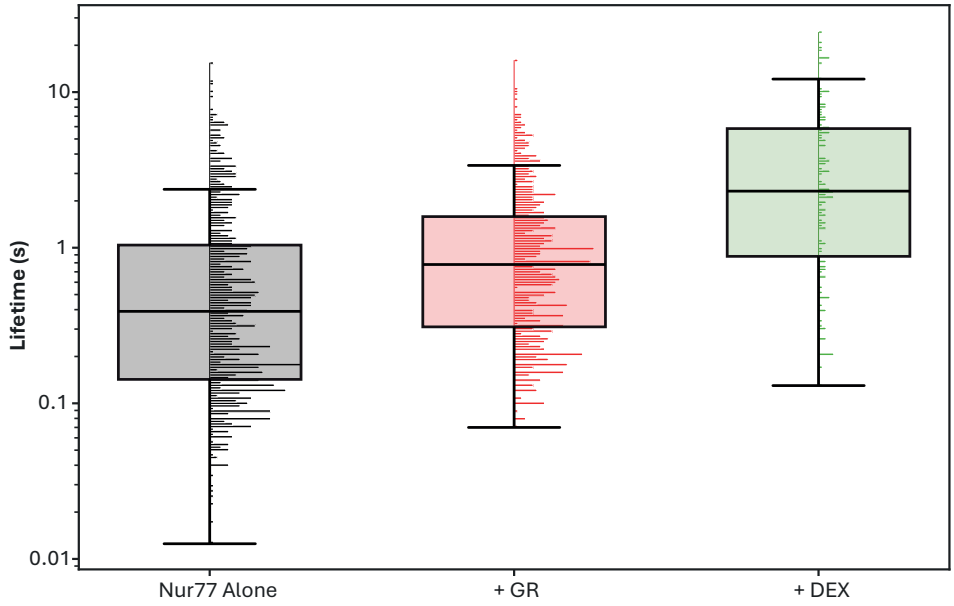

Figure S5. Boxplot with attached normalised histograms of the molecular lifetimes. *(Dex activated) GR and Dex significantly increases Nur77 lifetimes on DNA (Mann–Whitney U test, $p < 0.001$).*

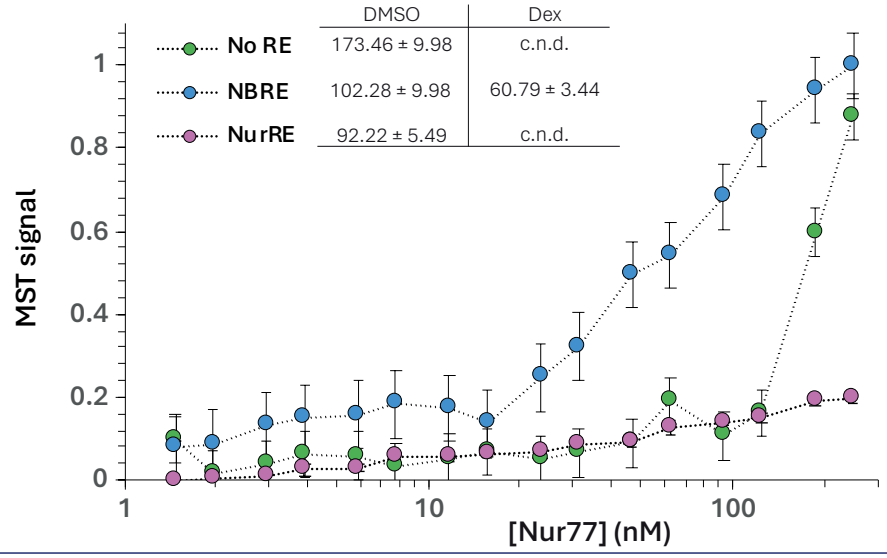

Figure S6. MST results of Nur77 binding to DNA sequences without a recognition sequence (No RE), the NBRE or the NurRE sequences. *Graph shows results for Nur77 with Dex. Error bars indicate the standard deviation of three independent measurements. Dashed lines are lines to guide the eye. Inset shows k_D values and errors were extracted from the binding fits for DMSO and Dex conditions on different DNA substrates. c.n.d. = k_D cannot reliably be determined.*